Current Optics and Photonics
Vol. 2, No. 6, December 2018, pp. 514-518

ISSN: 2508-7266(Print) / ISSN: 2508-7274(Online)
DOI: https://doi.org/10.3807/COPP.2018.2.6.514

Direct Measurement of Diffusion Length in Mixed Lead-halide Perovskite Films Using Scanning Photocurrent Microscopy

Ahram Kim[1,2], Byung Hee Son[1], Hwan Sik Kim[1], and Yeong Hwan Ahn[1]*

[1]*Department of Physics and Department of Energy Systems Research, Ajou University, Suwon 16499, Korea*
[2]*Gyeongbuk Software Convergence Promotion Center, Pohang Technopark, Pohang 37668, Korea*

(Received October 8, 2018 : revised November 7, 2018 : accepted November 7, 2018)

Carrier diffusion length in the light-sensitive material is one of the key elements in improving the light-current conversion efficiency of solar-cell devices. In this paper, we measured the carrier diffusion length in lead-halide perovskite ($MAPbI_3$) and mixed lead-halide ($MAPbI_{3-x}Cl_x$) perovskite devices using scanning photocurrent microscopy (SPCM). The SPCM signal decreased as we moved the focused laser spot away from the metal contact. By fitting the data with a simple exponential curve, we extracted the carrier diffusion length of each perovskite film. Importantly, the diffusion length of the mixed-halide perovskite was higher than that of the halide perovskite film by a factor of 3 to 6; this is consistent with the general expectation that the carrier mobility will be higher in the case of the mixed lead-halide perovskites. Finally, the diffusion length was investigated as a function of applied bias for both samples, and analyzed successfully in terms of the drift-diffusion model.

Keywords : Perovskites, Diffusion length, Scanning photocurrent microscopy
OCIS codes : (040.5350) Photovoltaic; (160.5335) Photosensitive materials; (310.3840) Materials and process characterization; (230.0250) Optoelectronics

I. INTRODUCTION

Lead-halide perovskites ($MAPbI_3$) have attracted substantial attention as one of the most promising materials for use in high-performance solar-cell devices, due to high carrier mobility, strong absorption across the solar spectrum, and simplicity of device fabrication [1-6]. Recently their efficiency has soared to 22.1%, despite being first developed in 2009, whereas there will be plenty of room for further improvement, considering the high electron-conversion efficiency of the light-absorbing perovskite materials [7-9]. However, total cell efficiency is still lower than for conventional silicon-based solar cells, and the key elements to improving cell efficiency lie in the development of optimized fabrication processes [10]. One of the key parameters is the diffusion length of the photogenerated carriers in the halide perovskite films, because charge-collection efficiency is dominated by the carrier-diffusion process.

The investigation of diffusion length in $MAPbI_3$ and its derivatives has been addressed indirectly using carrier lifetime measurements [1-3, 11-16]. In addition, using PL-scanned confocal microscopy, diffusion lengths of 14 μm and 6 μm have been measured for $MAPbI_3$ and $MAPbBr_3$ respectively [16]. Recently, scanning photocurrent microscopy (SPCM) has been proven to be a very effective tool for addressing the diffusion length in dye-sensitized solar cells (DSCs), without the knowledge of additional optical or transport parameters [17, 18]. Diffusion lengths of ~100 μm have been reported for conventional DSCs, and, more importantly, their correlation with the total cell efficiencies has been demonstrated explicitly. More recently, SCPM has been successfully exploited to investigate diffusion length in perovskite films [19], but the transport properties of the mixed lead-halide perovskites have been largely unexplored. In addition, the modified diffusion length under the influence of applied bias has not been addressed so far.

*Corresponding author: ahny@ajou.ac.kr, ORCID 0000-0002-8563-076X
Color versions of one or more of the figures in this paper are available online.

Here we performed SPCM measurements to address the diffusion lengths of the two types of perovskite films (halide and mixed-halide) coated on metal electrodes. In addition, the diffusion lengths were found under different applied-bias conditions, and analyzed in terms of the drift-diffusion model.

II. RESULTS AND DISCUSSION

Figure 1(a) shows the device configuration for measuring diffusion length in a perovskite film. We fabricated the devices by coating $MAPbI_3$ and $MAPbI_{3-x}Cl_x$ films on quartz substrate containing the source and drain metal electrodes. The metal electrodes were embedded in the substrate to produce high-quality perovskite film, because metallic structures protruding from the substrate tend to cause irregular coating in the film. For this purpose, we used a photolithography technique including a wet-etching process (with buffered oxide etchant solution for 100 s) to produce a trench structure with a thickness of 100 nm before the metal evaporation. The metal electrodes (Cr/Au) were deposited from a thermal evaporator to a thickness of 100 nm, so that the metal film was completely embedded in the quartz substrate, as illustrated in Fig. 1(a). Next, we used a conventional solution-based spin-coating method to fabricate the lead-halide perovskite film in a nitrogen glove box. $MAPbI_3$ powder (purchased from One solution) was added to a mixture of γ-butyrolactone (GBL) and dimethyl sulfoxide (DMSO) (7:3 v/v) and stirred at 60°C for 12 h. The $MAPbI_3$ solution was spin-coated on a quartz substrate (15 × 15 × 1 mm) treated with UV-ozone cleaning. The spin-coating conditions were 2000 rpm for 60 s. The toluene solution (150 μL) was introduced dropwise onto the substrate during spin coating [20]. The sample was annealed on a hot plate at 100°C for 15 min, and the thickness of the resulting perovskite film was 250 nm. We also fabricated $MAPbI_{3-x}Cl_x$ films having a thickness of 180 nm, using the same procedures but with a solution with a 3:1 molar ratio of CH_3NH_3I:$PbCl_2$. The scanning electron microscopy images for $MAPbI_3$ and $MAPbI_{3-x}Cl_x$ films are shown in Figs. 1(b) and 1(c), which confirms the formation of continuous films.

We performed a conventional SPCM measurement with a focused laser at 532 nm with a spot size of 500 nm, and raster-scanned using galvanometer scanning mirrors [21, 22]. A representative SPCM image for the $MAPbI_3$ device is shown in Fig. 2(a), measured in a nitrogen-purged environment. The source-drain voltage (V_{DS}) was fixed at zero. The laser's intensity was 5 μW. Throughout the experiment, SPCM images were measured while the entire sample area was illuminated by a homemade solar simulator

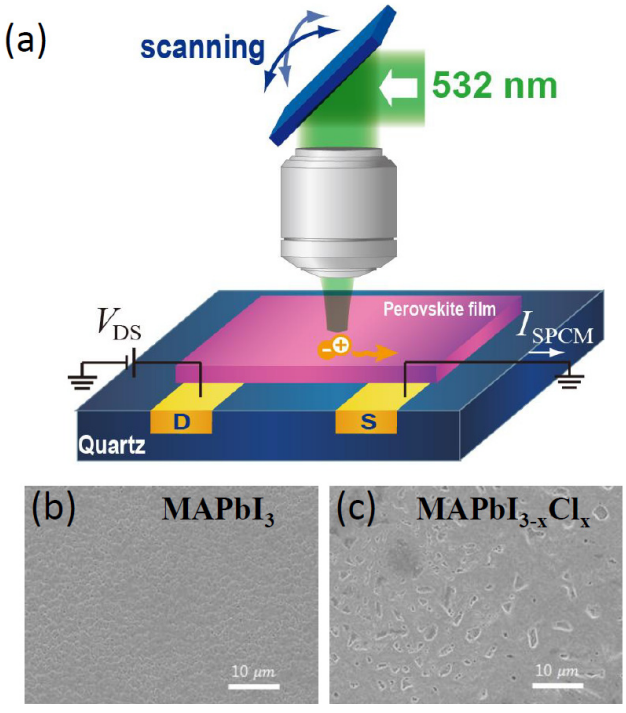

FIG. 1. (a) Schematic diagram of a perovskite device with drain and source electrodes embedded in a quartz substrate. For the diffusion-length measurement, we used a SPCM technique with a focused 532-nm laser. SEM images of (b) lead-halide and (c) mixed lead-halide perovskite films respectively.

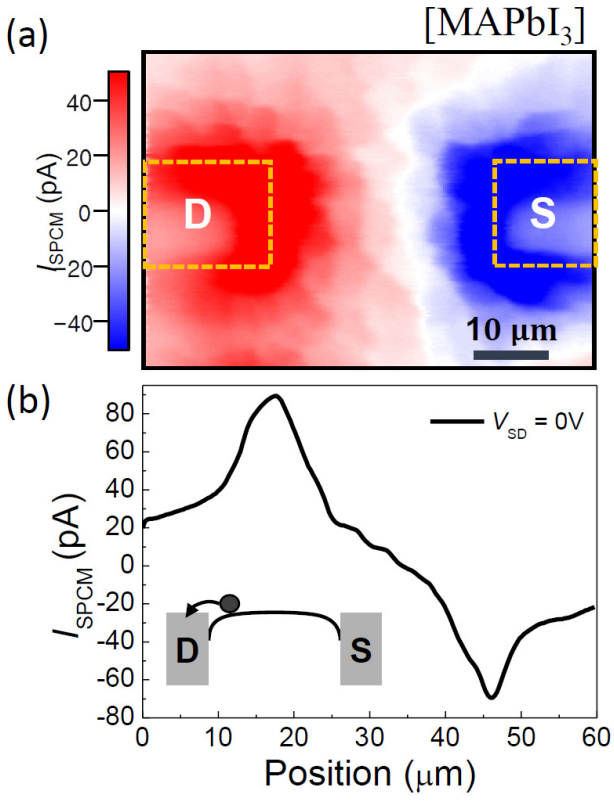

FIG. 2. (a) I_{SPCM} image of lead-halide perovskite film with a channel length of 30 μm. (b) Line profile of I_{SPCM} as a function of position along the channel, extracted from (a).

set at 1 sun [17]. The channel length l_{ch} and width w_{ch} of the device were 30 μm and 10 μm respectively. The scanning photocurrent signal I_{SPCM} was very strong near the metal contacts, and decreased gradually away from the metal electrodes [22-25]. We obtained positive and negative photocurrent near the drain and source electrodes respectively. This is more clearly shown in Fig. 2(b) by the I_{SPCM} line profile taken along the channel. In previous studies of semiconducting devices with nanowires, carbon nanotubes, graphene, and transition-metal dichalcogenide monolayers, the SPCM signals were generally dominated by the metallic signals, which originate from the Schottky barriers [24-26]. Accordingly, I_{SPCM} near the metal contacts will be dominated by the drift effects from the electric field in the contact areas. However, as the laser spot moves away from the contact region, I_{SPCM} tends to be dominated by the diffusion motion, as will be shown later. The polarity of I_{SPCM} indicates that the carriers collected by nearby electrodes are electrons, as shown in the inset of Fig. 2(b).

The SPCM signal is strongly modified under operating conditions, *i.e.* in the presence of an applied bais. Figure 3(a) shows a two-dimensional plot of I_{SPCM} as a function of laser-spot position and source-drain bias V_{DS}, for the mixed lead-halide device with $l_{ch} = 20$ μm. Here we recorded I_{SPCM} while we moved the laser position back and forth along the device's conduction channel (x-axis) and changed V_{DS} gradually (y-axis). As we applied V_{DS}, one of the metallic signals got stronger, whereas the signal at the opposite electrode was suppressed. For clarity, we show I_{SPCM} line profiles in Fig. 3(b), extracted from Fig. 3(a), for seven different V_{DS}'s. Clearly I_{SPCM} is stronger near the drain electrode for $V_{DS} > 0$, whereas it is stronger near the source electrode for $V_{DS} < 0$.

For a detailed analysis of the position-dependent I_{SPCM} line profiles, in Fig. 4(a), we show semilogarithmic plots of I_{SPCM} for different V_{DS} values, as a function of position x_0 measured from the metal's edge, for the device shown in Fig. 3. As mentioned, they are fitted well by a simple exponential decay function as x_0 gets larger. Starting from a two-dimensional diffusion model in the absence of electric field, the collected I_{SPCM} analytically leads to a simple one-dimensional exponential function for $x_0 > 0$, which is as follows:

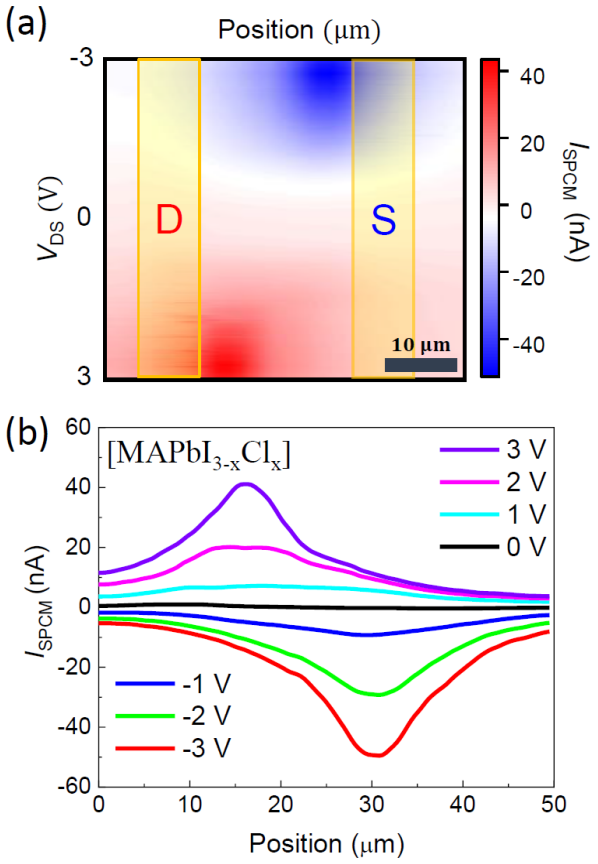

FIG. 3. (a) Two-dimensional plot of I_{SPCM} as a function of position (x-axis) and V_{DS} (y-axis) for a MAPbI$_{3-x}$Cl$_x$ device with channel length of 20 μm. (b) Line profiles of I_{SPCM} as a function of position, extracted from (a) for different values of V_{DS}.

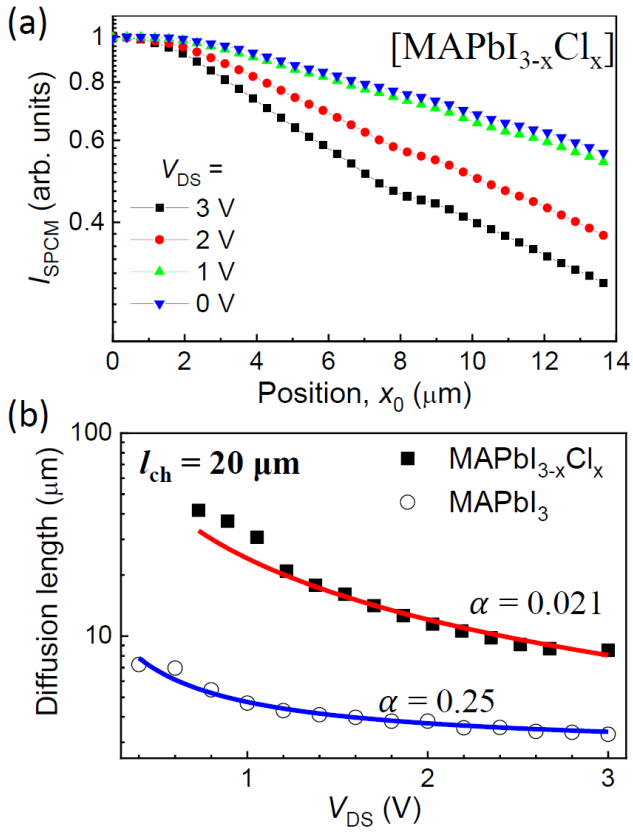

FIG. 4. (a) Semilogarithmic plots of I_{SPCM} as a function of position for different values of V_{DS}. (b) Diffusion length as a function of V_{DS}, for both MAPbI$_{3-x}$Cl$_x$ (filled boxes) and MAPbI$_3$ (open circles) devices with channel length of 20 μm. Solid lines are fits to the data based on the drift-diffusion model.

$$I_{SPCM} = \frac{eG}{2}\exp(-x_0 / L_n), \quad (1)$$

where e is the electron's charge, G is the electron-generation rate, and $L_n = \sqrt{D_n \tau_n}$ is diffusion length for electron diffusion coefficient D_n and electron lifetime τ_n [17]. Therefore, the diffusion length can be extracted explicitly by fitting I_{SPCM} using a simple exponential function, without requiring knowledge of the additional optical and transport parameters of the perovskites. We also note that this approach is advantageous compared to the aforementioned PL-scanned confocal microscopy, in which case information about the background carrier density and laser-induced carrier density is needed to estimate the diffusion length.

By fitting the data in Fig. 4(a), the diffusion length for the $MAPbI_{3-x}Cl_x$ device is plotted as a function of V_{DS} (filled boxes) in Fig. 4(b). For comparison, we added the results for a $MAPbI_3$ device as open circles. Importantly, the results indicate that the diffusion length in $MAPbI_{3-x}Cl_x$ is much larger, by a factor of 3 to 6, than in $MAPbI_3$, which is less than 10 μm [19, 27]. Although the mixed-halide perovskites have played a key role in the fabrication of solar cells with unprecedented, superior cell efficiency, the diffusion length for the mixed-halide films has not been demonstrated so far, especially using the SPCM technique.

In addition, it is clearly shown in Fig. 4(b) that the diffusion length varied dramatically with V_{DS}, for both $MAPbI_3$ and $MAPbI_{3-x}Cl_x$. The diffusion length for $MAPbI_{3-x}Cl_x$ was measured at 50 μm near $V_{DS} = 0$ V and decreased as V_{DS} increased, yielding 8.5 μm for $V_{DS} = 3$ V. Similarly, for $MAPbI_3$ it decreased from 8.5 μm at $V_{DS} =$ 0 to 3.3 μm at $V_{DS} = 3$ V. The diffusion length under the influence of an electric field has been addressed in other solar-cell systems, being well explained by the drift-diffusion model [17]. The field-dependent decay length L_{dec} (referred to as *decay lengths*, owing to the combined contribution from the drift effect) in an electric fields $\vec{E} = E\hat{x}$ (with $E < 0$, for electrons under $V_{DS} > 0$), leads to:

$$\frac{1}{L_{dec}} = -\frac{\mu_n}{2D_n}E + \sqrt{(\frac{\mu_n}{2D_n}E)^2 + (\frac{1}{L_n})^2} \approx -(19.53\ \mathrm{V}^{-1})E + \sqrt{(19.53\ \mathrm{V}^{-1})^2 E^2 + (\frac{1}{L_n})^2} \quad (2)$$

where μ_n is the carrier mobility, and we used the Einstein relation of $D_n / \mu_n = kT / e = 0.0256\,(V)$ at room temperature. From Eq. (2), it is evident that the decay length decrease with an increase of V_{DS}, as observed in our experiments. We note that this validates our approach for measuring the carrier diffusion length in perovskite films based on the SPCM technique. We also found similar behavior for devices with longer channel length ($l_{ch} = 250$ μm).

Here the effective electric field in the perovskite film can be expressed by $E = \alpha E_{ext}$, where α is a fractional coefficient and E_{ext} is the external electric field, *i.e.* V_{DS} divided by the channel length (20 μm). Our results in Fig. 4(b) are fitted using Eq. (2), yielding $\alpha = 0.25$ for $MAPbI_3$ and $\alpha = 0.021$ for $MAPbI_{3-x}Cl_x$. In this manner we could determine the effective electric fields induced in the perovskite layers that contribute to the transport of the photogenerated carriers. We note that the value for α is smaller in the case of the mixed-halide device, implying that its metal-perovskite contact is relatively poor. More importantly, because the mobility scales as L_n^2 (*i.e.* as $\mu_n = eL_n^2 / \tau_n kT$), one can expect that the mobility of the mixed-halide film will be higher than that of $MAPbI_3$ by more than a factor of 10. Future investigation will be required for a thorough understanding of the carrier transport phenomena in perovskite films, for instance, by measuring the carrier lifetimes in the films to estimate the mobilities of films with different chemical compositions.

III. CONCLUSION

We measured the carrier diffusion lengths in halide and mixed-halide perovskite films, using scanning photocurrent microscopy. The localized photocurrent signal decreased as we moved the focused laser spot away from the metal contact, from which we extracted the carrier diffusion length in both types of perovskite film. Importantly, the diffusion length in the mixed-halide perovskite is much higher than that in halide perovskite film, by a factor of about 3 to 6, which is consistent with the fact that mixed-halide perovskite film delivers larger photocurrent generation and increased cell efficiency. The SPCM signal was recorded as a function of the source-drain bias, for both samples. The bias-dependent diffusion lengths exhibited a decreasing tendency with increasing bias, which is consistent with the drift-diffusion model, allowing us to extract the effective electric fields inside the films. These results will trigger future study of the diffusion lengths in perovskite films and their derivatives with different chemical compositions and various morphologies. Our approach will provide an important guideline for interrogating carrier transport phenomena in various photovoltaic devices, to optimize cell efficiency.

ACKNOWLEDGMENT

This work was supported by the Midcareer Researcher Program (2017R1A2B4009177) through a National Research Foundation grant funded by the Korea Government (MSIP) and by the Human Resources Program in Energy Technology (20164030201380) of the Korea Institute of Energy Technology Evaluation and Planning (KETEP) grant, funded by the Korea Government (MOTIE).

REFERENCES

1. L. M. Herz, "Charge-carrier mobilities in metal halide perovskites: fundamental mechanisms and limits," ACS Energy Lett. **2**, 1539-1548 (2017).
2. S. D. Stranks, G. E. Eperon, G. Grancini, C. Menelaou, M. J. P. Alcocer, T. Leijtens, L. M. Herz, A. Petrozza, and H. J. Snaith, "Electron-hole diffusion lengths exceeding 1 micrometer in an organometal trihalide perovskite absorber," Science **342**, 341-344 (2013).
3. Q. Dong, Y. Fang, Y. Shao, P. Mulligan, J. Qiu, L. Cao, and J. Huang, "Electron-hole diffusion lengths >175 μm in solution-grown $CH_3NH_3PbI_3$ single crystals," Science **347**, 967-970 (2015).
4. H. J. Snaith, "Perovskites: The emergence of a new era for low-cost, high-efficiency solar cells," J. Phys. Chem. Lett. **4**, 3623-3630 (2013).
5. M. A. Green, A. Ho-Baillie, and H. J. Snaith, "The emergence of perovskite solar cells," Nat. Photon. **8**, 506-514 (2014).
6. C. Wehrenfennig, G. E. Eperon, M. B. Johnston, H. J. Snaith, and L. M. Herz, "High charge carrier mobilities and lifetimes in organolead trihalide perovskites," Adv. Mater. **26**, 1584-1589 (2014).
7. Y. Jeong, J. K. Sahu, D. N. Payne, and J. Nilsson, "Ytterbium-doped large-core fibre laser with 1 kW of continuous-wave output power," Electron. Lett. **40**, 470-472 (2004).
8. Y. Jeong, J. K. Sahu, D. N. Payne, and J. Nilsson, "Ytterbium-doped large-core fiber laser with 1.36 kW continuous-wave output power," Opt. Express **12**, 6088-6092 (2004).
9. U. Keller, "Recent developments in compact ultrafast lasers," Nature **424**, 831-838 (2003).
10. W. Nie, H. Tsai, R. Asadpour, J. C. Blancon, A. J. Neukirch, G. Gupta, J. J. Crochet, M. Chhowalla, S. Tretiak, M. A. Alam, H. L. Wang, and A. D. Mohite, "High-efficiency solution-processed perovskite solar cells with millimeter-scale grains," Science **347**, 522-525 (2015).
11. G. Hodes and P. V. Kamat, "Understanding the implication of carrier diffusion length in photovoltaic cells," J. Phys. Chem. Lett. **6**, 4090-4092 (2015).
12. Y. Yamada, T. Nakamura, M. Endo, A. Wakamiya, and Y. Kanemitsu, "Photocarrier recombination dynamics in perovskite $CH_3NH_3PbI_3$ for solar cell applications," J. Am. Chem. Soc. **136**, 11610-11613 (2014).
13. V. D'Innocenzo, A. R. Srimath Kandada, M. De Bastiani, M. Gandini, and A. Petrozza, "Tuning the light emission properties by band gap engineering in hybrid lead halide perovskite," J. Am. Chem. Soc. **136**, 17730-17733 (2014).
14. S. D. Stranks, V. M. Burlakov, T. Leijtens, J. M. Ball, A. Goriely, and H. J. Snaith, "Recombination kinetics in organic-inorganic perovskites: excitons, free charge, and subgap states," Phys. Rev. Appl. **2**, 034007 (2014).
15. E. Alarousu, A. M. El-Zohry, J. Yin, A. A. Zhumekenov, C. Yang, E. Alhabshi, I. Gereige, A. Alsaggaf, A. V. Malko, O. M. Bakr, and O. F. Mohammed, "Ultralong radiative states in hybrid perovskite crystals: compositions for submillimeter diffusion lengths," J. Phys. Chem. Lett. **8**, 4386-4390 (2017).
16. W. Tian, C. Zhao, J. Leng, R. Cui, and S. Jin, "Visualizing carrier diffusion in individual single-crystal organolead halide perovskite nanowires and nanoplates," J. Am. Chem. Soc. **137**, 12458-12461 (2015).
17. J. K. Park, J. C. Kang, S. Y. Kim, B. H. Son, J. Y. Park, S. Lee, and Y. H. Ahn, "Diffusion length in nanoporous photoelectrodes of dye-sensitized solar cells under operating conditions measured by photocurrent microscopy," J. Phys. Chem. Lett. **3**, 3632-3638 (2012).
18. J. D. Park, B. H. Son, J. K. Park, S. Y. Kim, J. Y. Park, S. Lee, and Y. H. Ahn, "Diffusion length in nanoporous TiO_2 films under above-band-gap illumination," AIP Adv. **4**, 067106 (2014).
19. S. Liu, L. Wang, W. C. Lin, S. Sucharitakul, C. Burda, and X. P. A. Gao, "Imaging the long transport lengths of photo-generated carriers in oriented perovskite films," Nano Lett. **16**, 7925-7929 (2016).
20. N. J. Jeon, J. H. Noh, Y. C. Kim, W. S. Yang, S. Ryu, and S. I. Seok, "Solvent engineering for high-performance inorganic-organic hybrid perovskite solar cells," Nat. Mater. **13**, 897-903 (2014).
21. J. K. Park, B. H. Son, J. Y. Park, S. Lee, and Y. H. Ahn, "High-speed scanning photocurrent imaging techniques on nanoscale devices," Curr. Appl. Phys. **13**, 2076-2081 (2013).
22. J. H. Yoon, H. J. Jung, J. T. Hong, J. Y. Park, S. Lee, S. W. Lee, and Y. H. Ahn, "Electronic band alignment at complex oxide interfaces measured by scanning photocurrent microscopy," Sci. Rep. **7**, 3824 (2017).
23. J. Park, Y. H. Ahn, and C. Ruiz-Vargas, "Imaging of photo-current generation and collection in single-layer graphene," Nano Lett. **9**, 1742-1746 (2009).
24. B. H. Son, J. K. Park, J. T. Hong, J. Y. Park, S. Lee, and Y. H. Ahn, "Imaging ultrafast carrier transport in nanoscale field-effect transistors," ACS Nano **8**, 11361-11368 (2014).
25. Y. C. Kim, V. T. Nguyen, S. Lee, J. Y. Park, and Y. H. Ahn, "Evaluation of transport parameters in MoS_2/graphene junction devices fabricated by chemical vapor deposition," ACS Appl. Mater. Interfaces **10**, 5771-5778 (2018).
26. Y. H. Ahn, A. W. Tsen, B. Kim, Y. W. Park, and J. Park, "Photocurrent imaging of p-n junctions in ambipolar carbon nanotube transistors," Nano Lett. **7**, 3320-3323 (2007).
27. Y. Li, W. Yan, Y. Li, S. Wang, W. Wang, Z. Bian, L. Xiao, and Q. Gong, "Direct observation of long electron-hole diffusion distance in $CH_3NH_3PbI_3$ perovskite thin film," Sci. Rep. **5**, 14485 (2015).